Published in final edited form as:
Anal Chem. 2009 August 15; 81(16): 6929–6935. doi:10.1021/ac901008c.

High-resolution temperature-concentration diagram of α-synuclein conformation obtained from a single Förster resonance energy transfer image in a microfluidic device

Virginia Vandelinder[†], **Allan Chris M. Ferreon**[§], **Yann Gambin**[§], **Ashok A. Deniz**[§,*], and **Alex Groisman**[†,*]

[†]Department of Physics, University of California, San Diego, 9500 Gilman Dr., MC 0374, La Jolla CA, 92093

[§]Department of Molecular Biology, The Scripps Research Institute, 10550 N. Torrey Pines Road, 92037 La Jolla, CA

Abstract

We present a microfluidic device for rapid and efficient determination of protein conformations in a range of medium conditions and temperatures. The device generates orthogonal gradients of concentration and temperature in an interrogation area that fits into the field of view of an objective lens with a numerical aperture of 0.45. A single Föster resonance energy transfer (FRET) image of the interrogation area containing a dual-labeled protein provides a 100×100 point map of the FRET efficiency that corresponds to a diagram of protein conformations in the coordinates of temperature and medium conditions. The device is used to explore the conformations of α–synuclein, an intrinsically disordered protein linked to Parkinson's and Alzheimer's diseases, in the presence of a binding partner, the lipid-mimetic sodium dodecyl sulfate (SDS). The experiment provides a diagram of conformations of α–synuclein with 10,000 individual data points in a range of 21 – 47 °C and 0 – 2.5 mM SDS. The diagram is consistent with previous reports, but also reveals new conformational transitions that would be difficult to detect with conventional techniques. The microfluidic device can potentially be used to study other biomolecular and soft-matter systems.

The crowded cellular milieu in which proteins manifest their biological activity is complex, involving numerous variables and interactions that can modulate and regulate protein structure and function. In order to understand how protein structure and function are controlled by the environment, biochemists and biophysicists routinely perform experiments where one chemical or physical parameter, such as ligand concentration or temperature, is varied, while other parameters are kept constant. The repetition of this "one-dimensional" experiment at a series of values of a second parameter can provide a two-dimensional (2D) phase diagram of the protein. However, because of the high material, labor, and time cost, the number of tested values of the second parameter is normally quite limited, and facets of the phase diagram could be missed because of insufficient resolution. The experimental workload is increased even further when additional parameters of the protein environment are varied. Therefore, new tools and techniques that enhance the speed and convenience of variation of multiple parameters are required for studies of proteins and other complex biochemical and soft-matter systems.

New tools and techniques would be particularly helpful in the study of intrinsically disordered proteins (IDPs). This class of proteins exhibits little detectable structure in isolation, but often

*To whom correspondence should be addressed: agroisman@ucsd.edu, deniz@scripps.edu.

acquires ordered conformations upon interaction with cellular binding partners; hence, IDPs generally exhibit complex and rich phase behavior in a multi-dimensional parameter space.1 One such IDP is α–synuclein, a 140 amino acid protein that is enriched at pre-synaptic nerve terminals. α–Synuclein is linked with neurodegenerative disorders, including Parkinson's disease and Alzheimer's disease. Although the protein is relatively well-studied, its specific biological role is not fully understood. Upon binding to natural and synthetic phospholipid membranes, α–synuclein undergoes structural transitions and adopts α-helical conformations.2 Several studies have shown that helical structures are similarly induced in α-synuclein upon binding to micelles composed of sodium dodecyl sulfate (SDS), a widely-used phospholipids mimetic.3–5 The structure of α–synuclein bound to SDS has been investigated using circular dichroism (CD),3 electron paramagnetic resonance (EPR),6 and nuclear magnetic resonance (NMR).7 In experiments using far-UV CD that combined temperature ramps with SDS titration, five different α–synuclein conformations were identified and the transitions between conformations were mapped in the [SDS]-temperature plane.8 More detailed information on the structure of α–synuclein and on the complex connections between SDS binding and α–synuclein folding at room temperature have been recently revealed by single-molecule Föster resonance energy transfer (smFRET) microscopy.9

FRET microscopy (in particular smFRET) has become increasingly popular as an experimental method for investigating protein conformations.[10–14] FRET is the non-radiative transfer of excited-state energy from a donor to an acceptor fluorescent molecule. By measuring fluorescence intensities from the donor and acceptor molecules, I_a and I_d, the transfer efficiency, E_{FRET}, can be calculated as $E_{FRET}=\frac{I_a}{I_a+\gamma I_d}$ (where γ is a correction factor). E_{FRET} has a strong dependence on the distance between the two molecules, approaching 1 for short donor-acceptor distances and being near zero for long distances, with a typical cross-over distance of ~50 Å for single-molecule dye pairs. Therefore, for a protein with one amino acid labeled with a donor molecule and another amino acid labeled with an acceptor molecule, E_{FRET} can be translated into the distance between the two amino acids, providing direct information on the protein conformation. Probing protein folding with FRET is particularly well-suited for microfluidic experiments, because FRET measurements can be performed under a microscope and high-quality data can be obtained from very small amounts of protein or even single protein molecules. [11–13]

Microfluidics can greatly facilitate the determination of protein conformation diagrams (or other soft matter phase diagrams) by generating a large number of mixtures with different proportions of the components in separate micro-droplets[15] or micro-compartments16 on the chip using small amounts of reagents. Gradients of concentration that are spontaneously formed by diffusion between adjacent micro-compartments can provide some additional phase information.16, 17 Stable, continuous concentration profiles with linear, polynomial,[18, 19] or exponential shapes[20] can be made with specialized microchannel networks, which were originally developed for differential coating of substrates and for studies of chemotaxis. In addition, instead of varying the temperature in time to observe phases present at different temperatures, the temperature can be varied in space across a microfluidic chip by circulating water with different temperatures through two parallel tubes attached to the chip.[21] Cremer *et al*. used temperature gradients to study the precipitation of a synthetic polymer at different temperatures. [22, 23] They also presented a microfluidic device where a temperature gradient is applied orthogonally to a set of microchannels with a sigmoidal profile of concentration and used it to test fluorescence of fluorescein as a function of its concentration and temperature.[24]

Here we present a microfluidic device designed for rapid and comprehensive tests of the dependence of protein structure on temperature and medium conditions using FRET. The

interrogation area of the device is a 1×1.6 mm array of 100 parallel channels with a linear variation of medium conditions between the channels and linear variation of temperature along the channels. A single FRET micrograph of the interrogation area with a dual-labeled protein in the microchannels provides a 100×100 point map of the FRET efficiency, resulting in a detailed diagram of protein conformational states in the coordinates of temperature and medium conditions. The device is used to test the SDS binding-induced folding of α–synuclein in a range of 21 to 47 °C in temperature and 0 – 2.5 mM in SDS concentration, and high-resolution diagrams of α–synuclein conformation are obtained. While generally consistent with previously reported results, the diagrams reveal previously unobserved folding transitions that would be difficult to find with conventional methods.

EXPERIMENTAL SECTION

Design of the microfluidic device

The microfluidic device to study protein phase diagrams (Figure 1a) is made of a microfabricated polydimethylsiloxane (PDMS) chip sealed by a #1.5 microscope cover glass. The chip has two layers of channels, a flow layer and a temperature control layer, separated by a 50-μm-thick layer of PDMS. The flow layer has 8-μm-deep microchannels that are adjacent to the cover glass and filled with a protein solution. The temperature control layer, which is imbedded in the chip, consists of three separate 1-mm-deep channels for temperature-controlled water circulation. The flow layer has three inlets (marked as 0%, 50%, and 100% in Figure 1a) and one outlet. The flow layer microchannel network contains two major elements: a gradient generator and an array of 100 parallel 8-μm-wide interrogation channels spaced 8 μm apart, in which the FRET efficiency is measured.

The gradient generator is designed according to the principles described previously[20] and has 4 stages of mixing (Figure 1b,c). It has 33 mixing channels in the last (4^{th}) stage and generates a linear series of 33 concentrations from solutions with relative concentrations of 0, 50, and 100% fed to the three inlets of the device. The streams coming from the 33 mixing channels merge to create a flow with smooth linear concentration profile, which is then split between the 100 parallel interrogation channels (Figure 1c,d). The large number of the mixing channels facilitates rapid smoothing without deterioration of the large-scale linear concentration profile. Such deterioration would occur if streams with different concentrations were allowed to flow side-by-side over a long distance.[20] To prevent this deterioration, the merging area is made short and the interrogation area is partitioned into an array of separate channels.

The gradient of temperature in the interrogation area was created by circulation of hot and cold water through two parallel channels that were oriented orthogonally to the interrogation channels in the flow layer (Figure 1d). The two circulation channels have a depth of 1 mm and are located 1 mm apart. A third channel in the temperature control layer, which was situated closer to the flow layer inlets, was used to circulate room-temperature water, thus isolating the gradient generator from any thermal effects from the cold and hot channels (Figure 1). The circulation channels were fabricated in PDMS25 (in contrast to Ref. 24 where brass tubes were used). The small length (~12 mm) and large depth of the circulation channels (as compared to ~0.25 mm in Ref. 25) led to low flow resistance and high volumetric flow rates at driving pressures provided by a standard laboratory circulators. The high flow rates were beneficial for setting well defined temperatures in the circulation channels. Our two-dimensional (2D) numerical simulations of the heat transfer in the device (Figure 1e and Supporting Information, Figure S1) indicated that the temperature profile in the 1-mm-wide interrogation area is nearly perfectly linear, with a range of temperatures of ~80% of the temperature difference between the cold and hot channels (Supporting Information, Figure S1d). Numerical simulations incorporating a 30 μm/s flow in the interrogation channels (as in our FRET experiments with protein solutions) showed that the perturbation of the temperature profile due to the flow was

negligible (<0.1% of the temperature difference between the cold and hot channels; see Supporting Information, Figure S1). Further details on the design of the microfluidic device are provided in Supporting Information.

Fabrication of the microfluidic devices

The microfluidic device was assembled from three layers of PDMS: a 50-μm-thick layer with flow channels, a 1-mm-thick layer with circulation channels, and a plain 4-mm-thick layer. The layers with flow and circulation channels were cast from two master molds that were fabricated using standard lithography techniques. The cast for the PDMS layer with circulation channels had 100 μm deep grooves for the bottom parts of the channels. The cast was cut by a razor blade all the way through along lines 100 μm away from the edges of the groves, thus forming 1 mm deep circulation channels with T-shaped cross-sections and lithographically defined edges (Figure 1e and Supporting Information, Figure S1a). Further details on the fabrication procedure are provided in Supporting Information.

Experimental set-up

All solutions fed to flow layer inlets and drawn off from the outlet were kept in 500 μL Eppendorf tubes and flow through the flow layer channels of the device was driven by setting a differential hydrostatic pressure between the inlets and outlets that was controlled within ~5 Pa using vertical rails and sliding stages. [20] The microfluidic device was mounted on a mechanical stage of a Nikon TE2000 inverted fluorescence microscope. The source of fluorescence illumination used for FRET microscopy and for measurements of the concentration profile in the interrogation area was a blue LED (royal blue Luxeon V by Lumileds, San Jose, CA; 700 mW with central wavelength 455 nm). The source of fluorescence illumination used for measurements of on-chip temperature was a cyan LED (cyan Luxeon V by Lumileds; 160 lm with central wavelength 505 nm). Each LED was mounted on a cooling fan and inserted into a modified Nikon lamp house. The LEDs were powered by a regulated DC supply and provided stable illumination with <0.5% variation in intensity over several hours. Fluorescence microscopy of fluorescein with the royal blue LED was performed using a standard FITC filter cube (Chroma, Rockingham, VT). Fluorescence microscopy with the cyan LED was performed using a filter set comprised of a 500/22nm excitation filter, 525nm dichroic mirror, and 550/50nm emission filter.

In FRET experiments, a 450/50nm excitation filter and a 505nm dichroic mirror were used. To capture images of two bands of FRET emission, we used two emission filters, 550/30nm for Alexa 488 donor dye and 620/60nm for Alexa 594 acceptor dye, which were held in a home-built slider. Images of the two bands were taken sequentially by manually changing the position of the slider. Although the time it took to switch emission filters was relatively large, it did not compromise the quality of imaging because of the stability of the LED illumination. Images of the interrogation area of the device were taken with a Nikon 10×/0.45 objective, a 0.42×Diagnostic Instruments relay lens and a Coolsnap HQ cooled digital camera (Photometrics, California). The field of view of the video microscopy setup was ~2.1×1.5 mm, with 0.25 mm margins around the 1.6×1 mm interrogation area. The resolution of the camera was 1.5 μm/pixel (the optical resolution was higher) with 5 pixels across each of the interrogation channels and 667 pixels along the interrogation channels from the cold to the hot circulation channel. Further details on the experimental setup are provided in Supporting Information.

Temperature control

The flow of water through the cold, hot, and room temperature circulation channels of the temperature control layer was driven by three different refrigerated circulators with digital displays, Haake F3, Fisher Scientific, and Lauda S, respectively. All circulator inlets and outlets

were connected to the respective inlets and outlets of the circulation channels through identically built lines of tubing, each consisting of a 5' long, 3/8" internal diameter (ID) tube connected to a 5" long, 1/16" ID tube connected to a segment of 16 gauge hypodermic tubing that was inserted into the device. The 3/8" ID segments were surrounded by foam pipe insulation. The volumetric flow rates through the cold, hot, and room-temperature circulation channels were measured with a graduated cylinder and were found to be 1.5 mL/s, 2.5 mL/s, and 0.5 mL/s, respectively. Those flow rates corresponded to mean flow velocities, $\bar{v}$, of 1.5 m/s, 2.5 m/s, and 1.2 m/s, and Reynolds numbers, *Re*, of ~1500, ~5000, and ~500, respectively (calculated as $\mathrm{Re} = \bar{v}d/\nu$ with channel widths, *d*, of 1, 1, and 0.4 mm and kinematic viscosities of water, ν, 0.001, 0.0005, and 0.001 Pa·s, respectively, for typical temperatures in the channels). Therefore, the flows in the cold and hot channels were expected to be turbulent, resulting in good mixing and uniform temperature at the channel boundaries. The temperatures in the hot and cold channel could be adjusted during experiments by changing the water temperature in the respective circulator.

The largest temperature difference between the cold and hot channels in our experiments (corresponding to the largest heat flux) was when water in the channels was at 15.5 and 53.5 °C, respectively. Our 2D FemLab numerical simulations for a room temperature of 20 °C (Supporting Information, Figure S1) indicated that the total heat flux through the walls of the cold and hot channels (each ~12 mm long) are 0.18 and 0.29 W, respectively. For water, which has a specific heat of 4.2 J/mL, with 1.5 and 2.5 mL/s flow rates, those heat fluxes were expected to result in respective water temperature changes of 0.02 and 0.03 °C. Therefore, the on-chip heat exchange was expected to have a negligible effect on the temperature in the circulation channels. The temperature in the 1/16" tubing connected to the circulation channel inlets and outlets was measured with an accuracy of 0.1 °C using a calibrated thermistor (121-104KAH-Q01 by Honeywell) encased in a section of the tubing. For the hot and cold circulators set at 55 and 15 °C, the temperature in the 1/16" inlet tubing lines differed by 1.2 and 0.4 °C from those inside the respective circulators. However, the differences in the water temperature between the 1/16" tubing lines connected to the inlet and outlet were only 0.4 and 0.1 °C for the hot and cold channel, respectively. Therefore, for the temperatures in the hot and cold circulation channels, we used the readings of the thermistors in the 1/16" inlet tubing with a −0.2 °C correction and no correction, respectively.

Protein Expression, Purification and Labeling

Mutagenesis of wild type α-synuclein (to generate a double cysteine, G7,84C, mutant), protein expression, and purification were carried out as previously described.[8, 9] Single-site labeling of the α-synuclein mutant with Alexa Fluor 488 maleimide (Invitrogen, Inc.), purification by HPLC, labeling with Alexa Fluor 594 maleimide, and final purification by HPLC provided dual-labeled protein for FRET measurements.

RESULTS

Before performing the FRET microscopy experiments, the temperature gradient and the distribution of concentrations in the interrogation area of the device were measured in a series of tests, in which aqueous solutions of fluorescein were fed to all device inlets. In all these tests and in the FRET experiments, the pressures in all three flow inlets were set at 2 kPa (8" of water column) above the outlet pressure. The resulting total flow rate through the device outlet was measured with a 5 μL Hamilton syringe at $2 \cdot 10^{-4}$ μL/s, corresponding to a mean flow velocity of 30 μm/s in each of the 100 interrogation channels.

The temperature gradient was characterized by feeding a 50 ppm solution of fluorescein in a 50 mM Tris buffer (pH 6.75 at room temperature) to all three inlets and taking fluorescence images of the interrogation area of the device with the cyan LED used as the light source. The

pH of the Tris buffer is temperature-dependent and decreases by ~0.028 units for each 1 °C increase in temperature. The fluorescence of fluorescein is strongly pH-dependent, with both absorption at 505 nm (the central wavelength of the LED) and the total emission decreasing by about a half from pH 7 to 6. Five reference images were taken with both hot and cold circulation channels fed by the same circulator at temperatures of 15, 25, 35, 45, and 55 °C, spanning the entire experimental range. (The temperature in the interrogation area was treated as uniform, because numerical simulations indicated that the temperature variations were always less than 0.25 °C.) The dependence of fluorescence on temperature was fitted with a 2^{nd} order polynomial, and the polynomial (together with the local values of fluorescence intensity at 15 °C) was used to calculate local temperatures from local fluorescence intensities when a temperature gradient was applied.

Because the temperature was not expected to vary across the interrogation channels (*x*-direction in Figure 1a), to reduce the measurement error, the values of fluorescence were averaged over 20 interrogation channels in the middle and over 10 μm (6.5 pixels) along the channels, resulting in 100 discrete data points along the gradient. A temperature profile measured with the hot and cold circulation channels at 50 and 12 °C, respectively, (Figure 2a) had a good linearity and was in good agreement with results of a numerical simulation without any adjustable parameters.

The distribution of concentrations in the interrogation channels was measured by feeding solutions of 0, 25, and 50 ppm fluorescein in a pH 7.5 phosphate buffer into the 0, 50, and 100% flow layer inlets, respectively. In this concentration range, the fluorescence of fluorescein in 8 μm deep channels is proportional to its concentration.[20] The diffusion coefficient of fluorescein (~$5\cdot10^{-6}$ cm^2/s), is close to that of SDS (~10^{-5} cm^2/s). Hence, the distribution of fluorescein was expected to be similar to that of molecular SDS in the FRET experiments. The distribution of fluorescein concentration was measured along a line about half-way between the circulation channels. The value of fluorescence in the middle of a channel averaged over 10 μm along the channel was taken as a representative. To compensate for non-uniformity of the illumination and light collection, the fluorescence distribution was normalized to a distribution obtained with all interrogation channels filled with a 50 ppm fluorescein solution. The measured distribution of concentration (Figure 2b) was close to the expected linear profile. The test was repeated with 0, 0.15, and 0.3% solutions of fluorescein-conjugated dextran (molecular weight ~77 kDa, ~1/60 fluorescein by mass; Sigma, St. Louis) fed to the 0, 50, and 100% inlets, and a similar linear concentration profile was obtained (not shown). The dextran diffusion coefficient, ~ $3\cdot10^{-7}$ cm^2/s, was comparable to that of SDS micelles. Therefore, we concluded that the micelle formation should not perturb the SDS concentration profile.

In the protein folding FRET experiment, the device inlets were fed with solutions containing 200 nM of the dual-labeled α-synuclein and 20 μM of unlabeled α-synuclein in a 0.2M NaCl, 10 mM NaH_2PO_4, 10 mM sodium acetate, 10 mM glycine, pH 7.50 buffer with SDS concentrations of 0, 1.25, and 2.5 mM for the 0%, 50%, and 100% inlets, respectively. Two FRET micrographs of the interrogation area were taken. The first micrograph was with the cold and hot circulation channels at 15.5 and 53.5 °C, respectively, and with a temperature range of 21 – 47 °C in the interrogation area. The second micrograph was for a 2 times narrower temperature range of 28 – 41 °C, with the hot and cold circulation channels at 25 and 44 °C. The values of E_{FRET} obtained from the central pixels of images of individual interrogation channels were averaged over 10 μm long segments along the channels, producing 100×100 point diagrams of E_{FRET} in the coordinates of [SDS] and temperature (Figure 3b,c). The diagram measured in the 28 – 41 °C temperature range (Figure 3c) was consistent with the diagram in the 21 – 47 °C range (Figure 3b).

The FRET diagrams directly demonstrate the complex folding pathway for α-synuclein which exhibits multiple equilibrium intermediates. The translation of the FRET diagrams into α-synuclein conformations is based on the previous studies with EPR, NMR, CD, and FRET. At room temperature and at [SDS] < 0.5 mM, α–synuclein primarily exists in its unstructured form (U-state), characterized by an intermediate distance between the fluorescent probes at amino acids 7 and 84, resulting in $E_{FRET} \approx 0.45$.[9] At [SDS] > 0.5 mM, helices form in the N-terminal and central regions of the protein, with a pronounced kink between the two helical sections (I-state),[5] resulting in a short distance between amino acids 7 and 84 and a high FRET efficiency, $E_{FRET} \approx 0.9$. A higher [SDS] of ~1 mM induces a shift to a fully extended helical structure (F-state), where amino acids 7 and 84 are far apart and $E_{FRET} \approx 0$. Above [SDS] ≈ 1.5 mM, most SDS molecules are in micelles and α-synuclein binds to the micelles, again adopting a kinked configuration (I_m-state) with a small distance between the labeled amino acids and $E_{FRET} \approx 0.9$.

A map of the α-synuclein conformational states on the [SDS]-temperature plane was obtained in a previous study[8] that tested a limited number of SDS concentrations and used temperature ramps and circular dichroism measurements to identify 50% population transition points (midpoints) between two different folding states. The transition midpoints reported in Ref. 8 and lines connecting the midpoints are plotted in Figure 3b. They are in reasonable agreement with transition lines between bordering states on the FRET diagram, which can be identified as lines connecting points with E_{FRET} values at arithmetic averages between those of the two states. (For transitions between the U- and I-states and between the I- and F-states in Figure 3b,c, the transition lines correspond to yellow strips.) However, the resolution and level of details in the FRET diagrams in Figure 3 are substantially higher than the resolution of the protein phase diagram from the previous study.[8] The enhanced resolution and the even coverage of the [SDS]-temperature phase space by the 100×100 grid make it possible to see a qualitatively new feature, which is a protrusion of the α-synuclein folding states with smaller distances between amino acids 7 and 84 (higher E_{FRET}) into the F-domain ($E_{FRET} \approx 0$) and an effective splitting of the F-state at [SDS] ≈ 1.3 mM and temperatures of 32 – 41 °C. The protrusion and the F-state splitting were consistently observed in all four FRET diagrams that we obtained on two different days (Figure 3b,c and data not shown). We note that this feature of the α-synuclein conformation diagram was not resolved in the previous studies and would be much more difficult and laborious to detect with conventional isothermal titration and temperature ramp techniques.

DISCUSSION AND CONCLUSIONS

The microfluidic device that we built and used in this study is advantageous compared to the previous designs in several respects. The fabrication of the water circulation channels by a combination of manual cutting and lithography made it possible to combine the large channel depth (1 mm) with accurate definition of channel boundaries (see Supporting Information, Figure S1). The large depth of the circulation channels that would be difficult to achieve purely lithographically (as in some previous studies[25, 26]) resulted in low hydrodynamic resistance, leading to a high flow rate and uniform temperatures inside the channels. In addition, the relatively small temperature differences between the tubing lines connected to the inlets and outlets made it possible to measure the temperature in the circulation channels using thermistors inserted in the tubing lines.

The accurate definition of the channel boundaries made it possible to apply a well defined temperature gradient over a relatively short distance of 1 mm, as compared to ~1 cm distances in some previous designs[21, 24], thus minimizing perturbations to the gradient due to heat exchange between the device and the air around it. Furthermore, because of the short distance between the circulation channels, the entire interrogation area fitted into the field of view of a

10x, NA = 0.45 objective lens. The relatively high numerical aperture of the objective provided good spatial resolution and efficient fluorescence illumination and light collection, making it possible to obtain high quality FRET images. Importantly, the optical interrogation was performed without moving the microscope stage or taking multiple images, which is an improvement over the previous studies with superimposed gradients of temperature and concentration.[15,24] Another feature of the device that enabled high-resolution phase diagrams to be obtained from single FRET micrographs was the array of 100 parallel 8 μm wide interrogation channels with a linear variation of the SDS concentration between the channels. For comparison, the previous design had only 10 channels and the concentration variation followed a sigmoidal curve.[24] The generation of the linear series of 100 concentrations was substantially facilitated by the use of the gradient generator of the type introduced in Ref. [20] that produced protein solutions with 33 concentrations of SDS out of 3 source solutions in just 4 steps. A modified version of the microfluidic device that we designed and tested in preliminary experiments (Supporting Information, Figure S2) generated an exponential series of 100 concentrations spanning a 256-fold range.

The application of the microfluidic device to mapping the conformational states of α-synuclein tested the experimental system on an intrinsically disordered protein with a rich folding repertoire and showcased the strengths of the presented system. A 2D phase diagram of α-synuclein, which required many days of careful experimentation to obtain by CD measurements in a cuvette with temperature ramps at different SDS concentrations in a previous study,[8] was obtained from a single FRET micrograph. The high resolution of the protein conformation diagram, which is equivalent to 10^4 individual data points, provided a substantially higher level of details on the α-synuclein folding states, making it possible to detect a new feature, a splitting of the folded (F) state at [SDS] ≈ 1.3 mM (Figure 3b,c). The F-state-splitting is observed in a complex region of the protein-SDS system, where at least three conformational states of α-synuclein and at least two assembly states (micelles and monomers) of SDS coexist, and may be a result of complex interactions of different assembly states of SDS with different conformations of α-synuclein.

In addition to saving time and providing enhanced resolution, the presented device and technique help avoid experimental errors resulting from performing experiments on different days over an extended period of time, including variability and aging of the protein sample and uncontrolled variations in the measurement setup. Another beneficial feature of the proposed experimental system is the possibility to “zoom-in” on specific regions of the phase space (particular intervals of temperature and [SDS]) after obtaining a relatively coarse diagram covering the entire relevant ranges of the two parameters. It is especially simple to enhance the resolution of the diagram in a specific range of temperatures, because this can be done on the fly by readjusting the water circulators, as exemplified by the diagram in Figure 3c that covers half of the temperature range of Figure 3b with twice the resolution.

We must note that the application of FRET as a method for detecting protein conformations requires dual-labeling of the protein molecules, which is a somewhat laborious process, involving multiple steps of labeling, testing, and purification. In addition, the attachment of fluorescent dyes and the preceding mutagenesis of the protein may potentially change its conformations. Nevertheless, this concern can be reduced and the sample preparation process can be substantially simplified by using singly-labeled protein molecules in conjunction with measurements of fluorescence intensity, polarization, and lifetime. Measurements of these parameters would provide diverse information about protein structure and they can all be performed in the presented microfluidic device. Moreover, the combination of these measurements and the measurements of FRET of dual-labeled proteins can potentially result in more detailed diagrams, making it possible to better distinguish between different protein conformations in complex systems.

In general, the rapid acquisition of broad-range phase diagrams in the microfluidic device using FRET or other fluorescence techniques can serve as a first step in detection of conformations, conformational transitions, and folding intermediates in new protein systems. The details of protein conformations in specific regions of the phase diagram can be subsequently studied using various conventional techniques (e.g., EPR, NMR, CD, or X-ray crystallography). The same techniques as well as single-molecule FRET detection in the microfluidic device can also be used in parameter ranges where multiple protein conformations are likely to co-exist, such as the F-state splitting region in the phase diagrams in Fig. 3b, c.

The rapid acquisition of phase diagrams with the microfluidic device can be especially advantageous for testing the interactions of intrinsically disordered proteins that often have multiple binding partners. For example, in the cell, α-synuclein is believed to interact with several ligands, which are expected to have substantial effects on the protein's structure and function; therefore, the proposed device can facilitate the analysis of the multidimensional space of α-synuclein interactions. The proximity of the labeled protein residues, as measured by FRET, can be translated into protein conformation, which can be directly related to the protein free energy. The residue proximity can also be readily compared with the results of numerical simulations of protein folding. Therefore, the detailed maps of protein folding states and boundaries between them in the temperature-concentration coordinates, as obtained with the microfluidic device, provide insight into the protein energy landscape and can help direct, improve, and validate numerical simulations.

While this study used a gradient of SDS, a lipid-mimetic protein binding partner, the same device can be used to produce other concentration gradients, including denaturant (e.g., guanidine hydrochloride or urea), pH, and osmolyte. Moreover, the presented device can potentially be applied to study protein-protein interactions, conformations of nucleic acids and their complexes with proteins, and synthetic soft matter systems.

Supplementary Material

Refer to Web version on PubMed Central for supplementary material.

Acknowledgments

We are grateful to Dr. Nelson B. Cole and Dr. Robert L. Nussbaum (National Institutes of Health, Bethesda, MD) for providing the plasmid construct for wild type α-synuclein. This work was supported by grant GM066833 from the National Institute of General Medical Sciences, NIH (A.A.D.), a postdoctoral fellowship from the National Institute of Neurological Disorders and Stroke, NIH (A.C.M.F.), and NSF grants OCE-0428900 and PHY0750049 (A.G., V.V., and A.A.D.).

References

1. Dyson HJ, Wright PE. Nature Reviews Molecular Cell Biology 2005;6:197–208.
2. Davidson WS, Jonas A, Clayton DF, George JM. Journal Of Biological Chemistry 1998;273:9443–9449. [PubMed: 9545270]
3. Weinreb PH, Zhen WG, Poon AW, Conway KA, Lansbury PT. Biochemistry 1996;35:13709–13715. [PubMed: 8901511]
4. Bussell R, Eliezer D. Journal Of Molecular Biology 2003;329:763–778. [PubMed: 12787676]
5. Ulmer TS, Bax A, Cole NB, Nussbaum RL. Journal Of Biological Chemistry 2005;280:9595–9603. [PubMed: 15615727]
6. Jao CC, Der-Sarkissian A, Chen J, Langen R. Proceedings Of The National Academy Of Sciences Of The United States Of America 2004;101:8331–8336. [PubMed: 15155902]
7. Eliezer D, Kutluay E, Bussell R, Browne G. Journal Of Molecular Biology 2001;307:1061–1073. [PubMed: 11286556]

8. Ferreon ACM, Deniz AA. Biochemistry 2007;46:4499–4509. [PubMed: 17378587]
9. Ferreon ACM, Gambin Y, Lemke EA, Deniz AA. Proceedings Of The National Academy Of Sciences Of The United States Of America 2009;106:5645–5650. [PubMed: 19293380]
10. Selvin PR. Nature Structural Biology 2000;7:730–734.
11. Deniz AA, Laurence TA, Beligere GS, Dahan M, Martin AB, Chemla DS, Dawson PE, Schultz PG, Weiss S. Proceedings Of The National Academy Of Sciences Of The United States Of America 2000;97:5179–5184. [PubMed: 10792044]
12. Schuler B, Lipman EA, Eaton WA. Nature 2002;419:743–747. [PubMed: 12384704]
13. Schuler B. Chemphyschem 2005;6:1206–1220. [PubMed: 15991265]
14. Deniz AA, Mukhopadhyay S, Lemke EA. Journal Of The Royal Society Interface 2008;5:15–45.
15. Song H, Ismagilov RF. Journal Of The American Chemical Society 2003;125:14613–14619. [PubMed: 14624612]
16. Hansen CL, Skordalakes E, Berger JM, Quake SR. Proceedings Of The National Academy Of Sciences Of The United States Of America 2002;99:16531–16536. [PubMed: 12486223]
17. Liedl T, Simmel FC. Analytical Chemistry 2007;79:5212–5216. [PubMed: 17563115]
18. Jeon NL, Dertinger SKW, Chiu DT, Choi IS, Stroock AD, Whitesides GM. Langmuir 2000;16:8311–8316.
19. Dertinger SKW, Chiu DT, Jeon NL, Whitesides GM. Analytical Chemistry 2001;73:1240–1246.
20. Campbell K, Groisman A. Lab on a Chip 2007;7:264–272. [PubMed: 17268630]
21. Mao HB, Yang TL, Cremer PS. JACS 2002;124
22. Mao HB, Li CM, Zhang YJ, Bergbreiter DE, Cremer PS. Journal Of The American Chemical Society 2003;125:2850–2851. [PubMed: 12617632]
23. Mao HB, Li CM, Zhang YJ, Furyk S, Cremer PS, Bergbreiter DE. Macromolecules 2004;37:1031–1036.
24. Mao HB, Holden MA, You M, Cremer PS. Analytical Chemistry 2002;74:5071–5075. [PubMed: 12380832]
25. Groisman A, Lobo C, Cho H, Campbell JK, Dufour YS, Stevens AM, Levchenko A. Nature Meth 2005;2:685–689.
26. Chung K, Cho JK, Park ES, Breedveld V, Lu H. Analytical Chemistry 2009;81:991–999. [PubMed: 19178337]

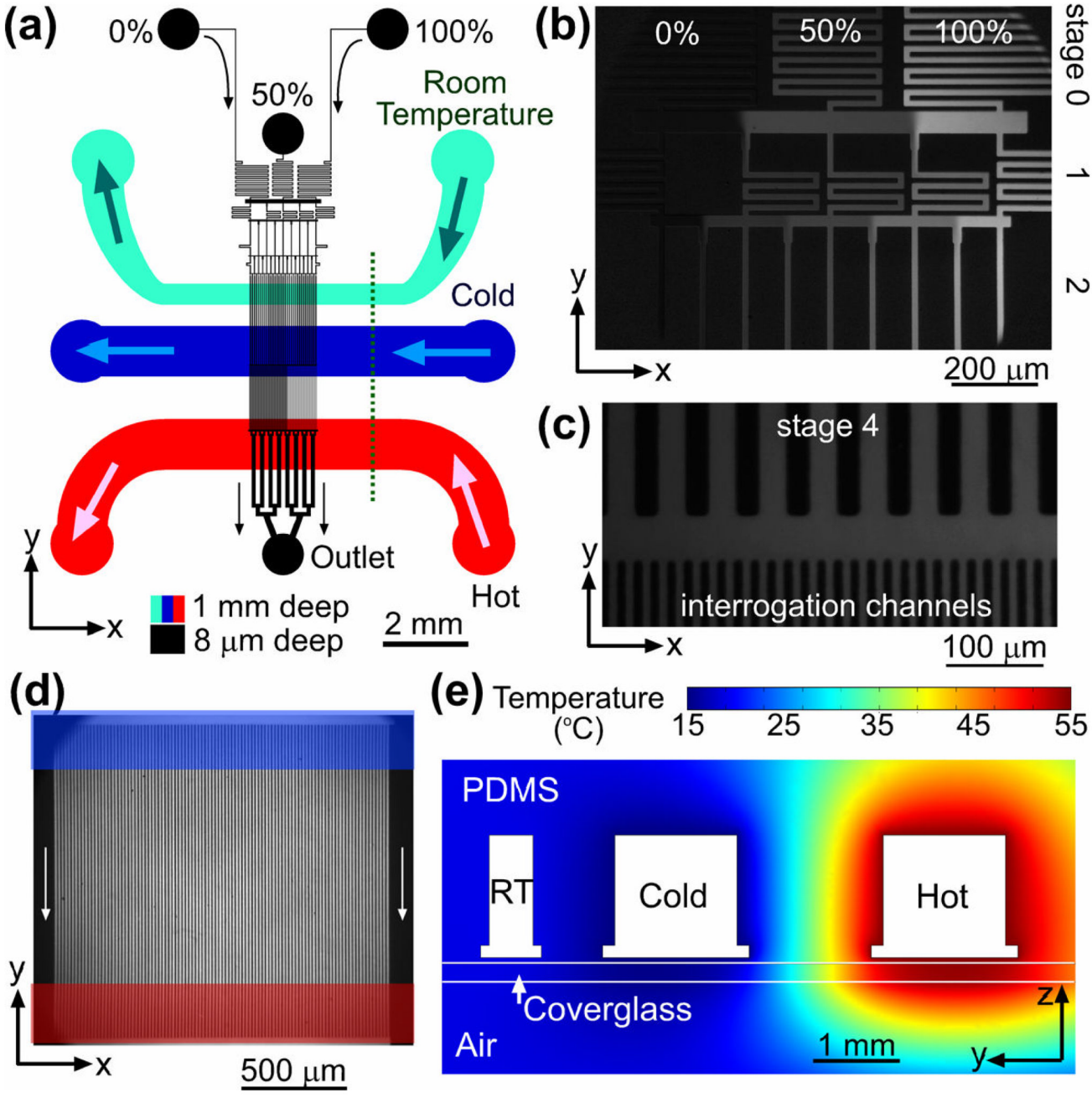

Figure 1.

Microfluidic device. **(a)** A schematic drawing of the microfluidic device. The flow channel network is shown in black. Three inlets of the device are labeled by the relative concentrations of the solutions fed to them, 0, 50, and 100%. The cyan, blue, and red channels (all 1 mm deep) are for circulation of room temperature, cold, and hot water, respectively. Arrows indicate flow directions. **(b)–(d)** Fluorescence micrographs of different parts of the gradient generator taken with 0, 25, and 50 ppm solutions of fluorescein in a pH 7.5 phosphate buffer fed to the 0, 50, and 100% inlets of the device, respectively. (b) Mixing channels of stages 0 – 2 and redistribution channels (horizontal strips) between them. (c) Mixing channels of stage 4 (25 μm wide straight channels with 25 μm partitions), a redistribution channel (horizontal strip),

and entrance parts of the interrogation channels (8 μm wide with 8 μm partitions). (d) Interrogation area of the device with 100 parallel channels (vertical strips). Locations of the cold and hot circulation channel are marked by a blue and red horizontal strip, respectively. **(e)** Cross-sectional view of the microfluidic device along the dotted line in (a) with color-coded temperature profile as obtained from a two-dimensional FEMLAB thermal conductivity simulation with the boundaries of the cold, room temperature (RT), and hot channels, at 15, 20, and 55 °C, respectively (see Supporting Information, Figure S1 for further details).

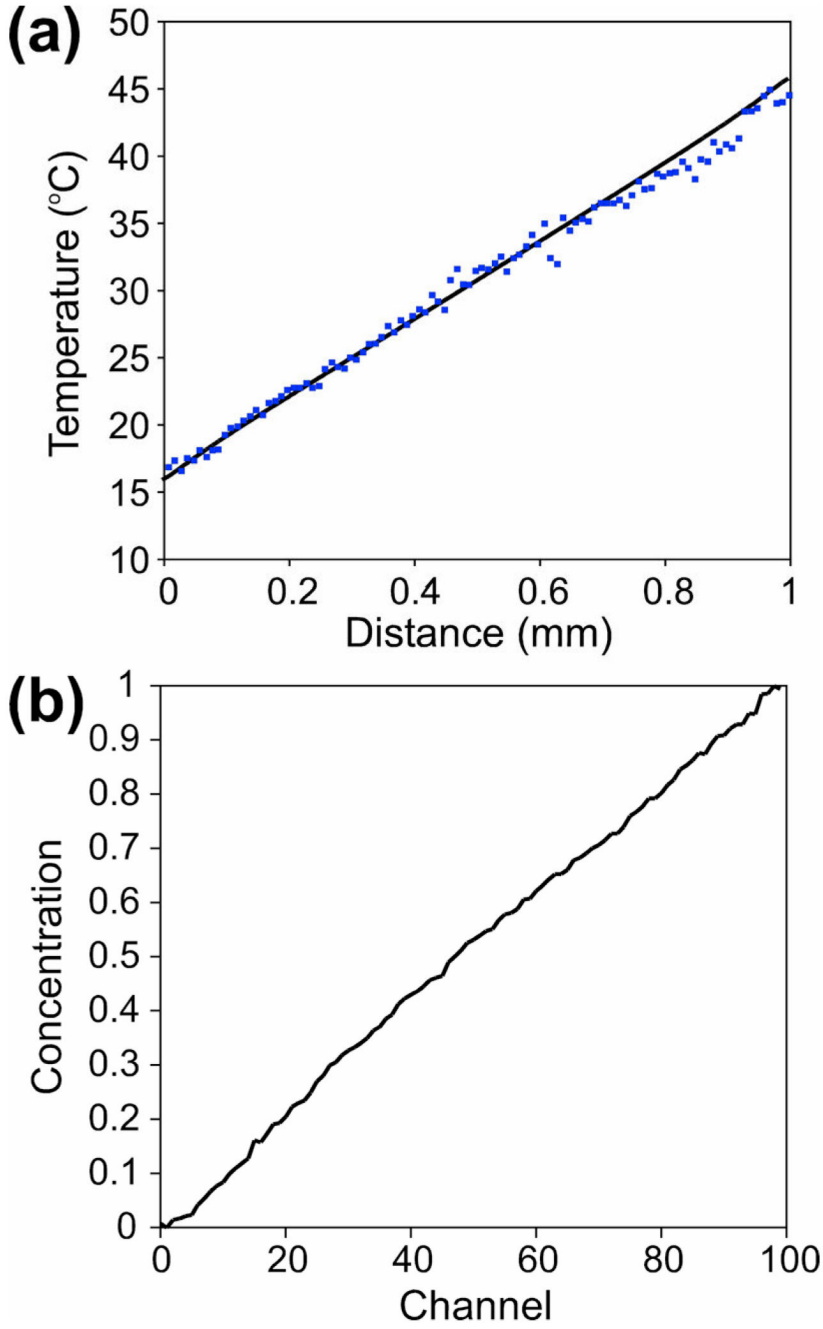

Figure 2.

(a) The temperature in the interrogation area of the device as a function of distance from the edge of the cold channel, with the cold and hot channels at 12 and 50 °C, respectively. Dots are experimental measurements; solid line is a FEMLAB numerical simulation with no fitting parameters. **(b)** Concentration of fluorescein (in relative units) in the interrogation channels as a function of channel number with 0, 25, and 50 ppm solution of fluorescein fed to the 0, 50, and 100% inlet, respectively. A concentration of 1 corresponds to a 50 ppm solution.

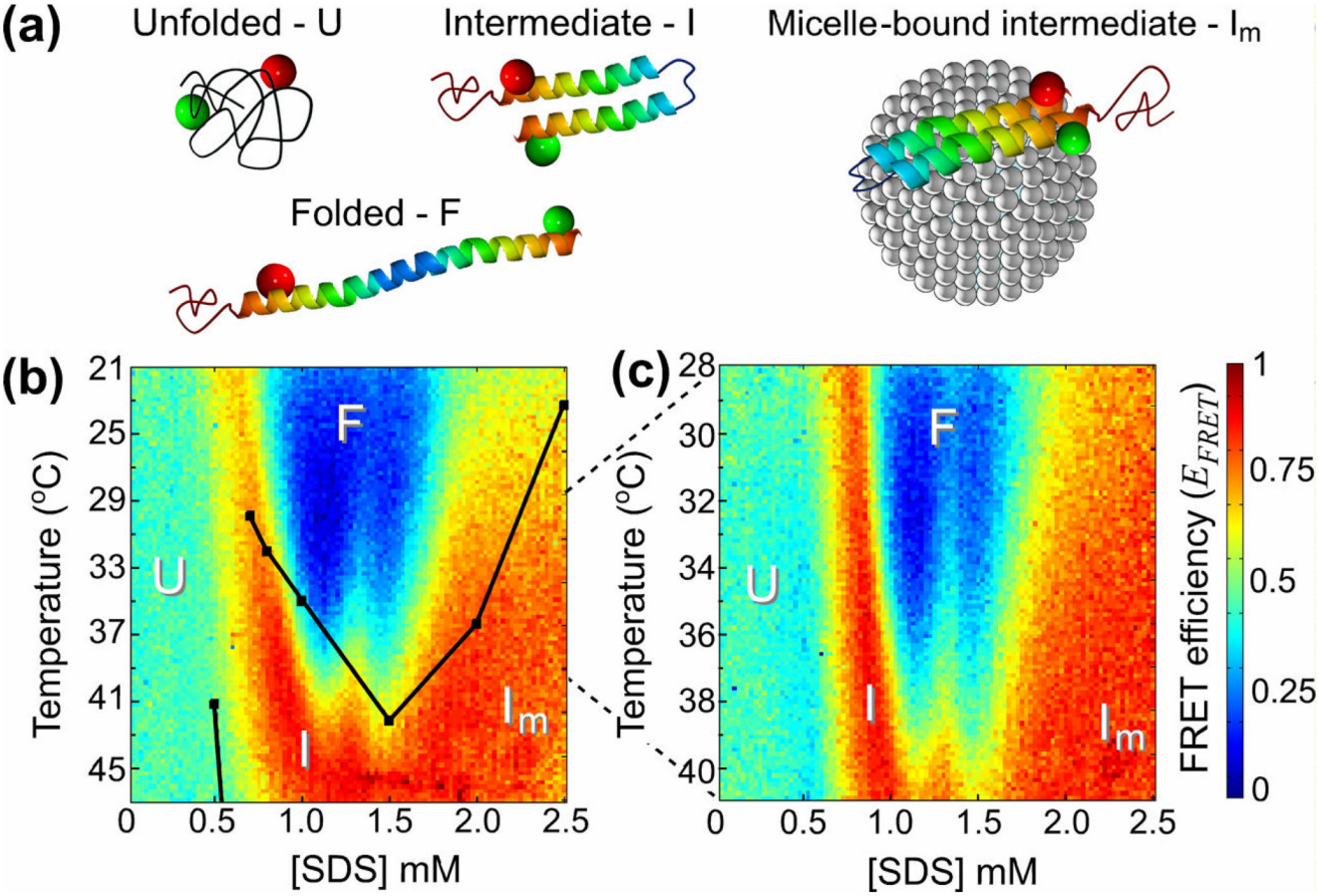

Figure 3.

(a) Schematic drawings of various conformational states of α-synuclein with a micelle bound to it in the I_m state. Green and red spheres indicate the fluorescent dyes, Alexa 488 and 594, respectively. **(b)–(c)** Color-coded diagrams of apparent FRET efficiency, E_{FRET}, as a function of SDS concentration, [SDS], and temperature, with the protein conformations, U, I, F, and I_m, assigned to different domains. Black dots in (b) designate the 50% two-state transition midpoints between different states from temperature ramp experiments in Ref. [8]. The dots are connected by lines to guide the eye. The temperature range in (c), 28 – 41°C, is half as broad as in (b), 21 – 47 °C.